Features of creating wear-resistant anti-corrosion coatings with a barrier layer on fragments of fuel claddings from E110 o.ch.

B A Kalin[1], A S Yashin[1], P S Dzhumaev[1], D A Safonov[1], E L Korenevsky[1], D A Fedorov[1], V V Novikov[2], V I Kuznetsov[2], P V Fedotov[2], V P Krivobokov[3], S N Yanin[3], A A Mokrushin[4], K K Polunin[4] and V V Uglov[1, 5]

[1] National Research Nuclear University MEPhI (Moscow Engineering Physics Institute), Kashirskoe highway 31, 115409 Moscow, Russia
[2] JSC «High-tech Research Institute of Inorganic Materials named after academician A.A Bochvar», Rogova street, 5a, 123098 Moscow, Russia
[3] National Research Tomsk Polytechnic University, Lenina avenue, 30, 634050 Tomsk, Russia
[4] LUCH Research and Production Association, Research and Development Institute, Federal State Unitary Enterprise, Zheleznodorozhnaya street, 24, 142100 Moscow region, Podolsk, Russia
[5] Belarusian State University, Nezavisimosti avenue, 4, 220030 Minsk, Republic of Belarus

E-mail: yashin_itf@mail.ru

Abstract. Results of the development of protective chromium-containing coatings based on the FeCrNi and CrNi systems for fuel claddings within framework of the accident tolerant fuel (ATF) are presented in this paper. Coatings were deposited by the outer surface of cladding tubes fragments from E110 o.ch. alloy (sponge-based Zr-1%Nb) up to 500 mm length by complex ion-plasma treatment on ILUR-03 and KVK-10 installations. The results of the control tests carried out in high-temperature steam at the GAZPAR bench at 1200 ºC up to 400 s showed that Cr-FeCrNi-Cr and Cr-CrNi-Cr coatings reduce total oxygen penetration into the alloy from 144 to 98 and 55 μm, respectively and Cr-CrNi-Cr coatings with a Mo barrier layer completely block the diffusion of oxygen into the material.

1. Introduction

One of the priority tasks of the world energy industry is to increase the lifetime of structural materials in WWER and PWR reactors cores in emergency conditions to increase safety level of its operation. Among the possible ways to improve fuel claddings to create the so-called tolerant fuel (ATF), stable in loss-of-coolant-accidents (LOCA), modification of surface layer of the material and protective coatings deposition by ion-plasma technologies is one of the most effective and technologically method. Researchers from different countries use various elements, alloys and compounds, such as Si, Cr, Al-Zr, FeCrAl, FeCrNi, TiAl, TiN, CrN, ZrN, however, chromium-containing coatings are mentioned as the most promising [1-5].

2. Materials and tools

Fragments of fuel claddings an external diameter of Ø9.1 mm and Ø9.5 mm up to 500 mm length made of alloy E110 o.ch. (sponge-based Zr-1% Nb) were used as samples for this research. Coatings were deposited by complex ion-plasma treatment on the ILUR-03 and KVK-10 installations (NRNU MEPhI, Department No. 9) operating in a semi-automatic mode [6, 7]. The treatment included the sequential execution of a series of operations: preliminary activation of the surface of Ar^+ ion beams E<1 keV; layer-by-layer deposition of coatings using magnetron sputtering systems; intermediate processing of Ar^+ ions with energies up to 35 keV using KVK-10 for surface doping with ion mixing mode [8, 9].

During processing at the ILUR-03 installation, shown at Figure 1 (a), the tubular sample was placed horizontally and sequentially moved through a vacuum chamber with an ion source into a chamber with 3 magnetrons mounted in the radial direction. In the KVK-10 installation, shown at Figure 1 (b), the samples are mounted vertically in a 6-seat cassette, which is placed in a vacuum chamber with 2 ion sources, 3 magnetrons and a high-energy ion implanter mounted on the periphery. The uniformity of processing is ensured by the stable operation of the devices, as well as by the control of the axial rotation speeds and the movement of the samples.

a) 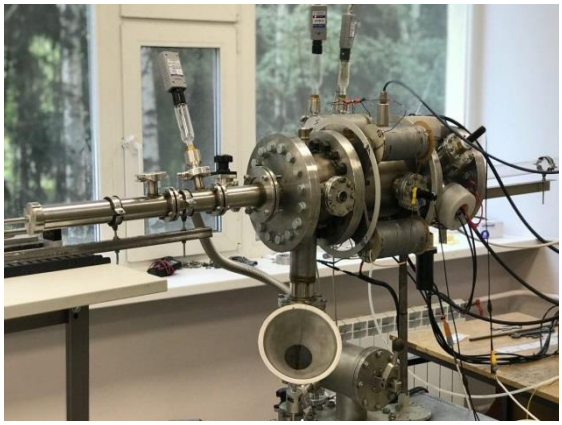 b) 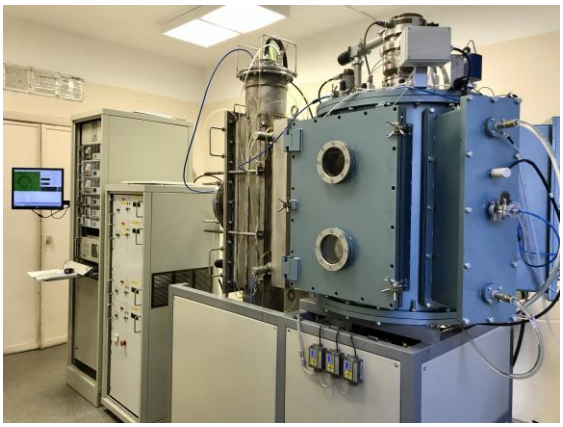

Figure 1. Photos of installations for complex ion-plasma surface treatment of materials ILUR-03 (a) and KVK-10 (b).

Corrosion testing of samples were carried out on the GAZPAR stand (LUCH FSUE) by isothermal exposure in water steam at 1200 ºC and subsequent cooling of the samples in argon atmosphere at least with 20° $C \cdot s^{-1}$ according to the procedure described in [10]. The corrosion degree was estimated by the specific weight gain and the local oxidation depth (ECR, %), which was calculated as the relative thickness of the zirconium layer, which would turn into oxide, provided that all the absorbed oxygen went into the formation of stoichiometric zirconium oxide ZrO_2.

The surface topography and the transverse structure of the samples in initial state and with coatings before and after high temperature tests were studied in scanning electronic microscopes Carl Zeiss EVO 50 and JEOL JSM-6610LV (resolution up to 3 nm). Both devices are equipped with X-ray microanalysis consoles for investigation of the elemental composition surface of the samples using an energy dispersive detector (EDS, Inca X-act) and a wave dispersive detector (WDS, Inca Wave 500).

3. Results and discussion

As preliminary experiments results shown (Figure 2) chrome coatings are prone to cracking and destruction under the influence of internal stresses arising during high-temperature oxidation in water steam due to thermal expansion and $\alpha \rightarrow \beta$ phase transformation in zirconium at ~800 ºC, due to the natural fragility of chromium. Among the disadvantages of chromium coatings, one should also note

the relatively high diffusion rate of Cr in Zr and the presence of a eutectic reaction at 1332 °C with, a brittle $ZrCr_2$ phase forming. In this regard, more plastic compositions of FeCrNi and CrNi in various element ratios were used as the basis of coatings in this work.

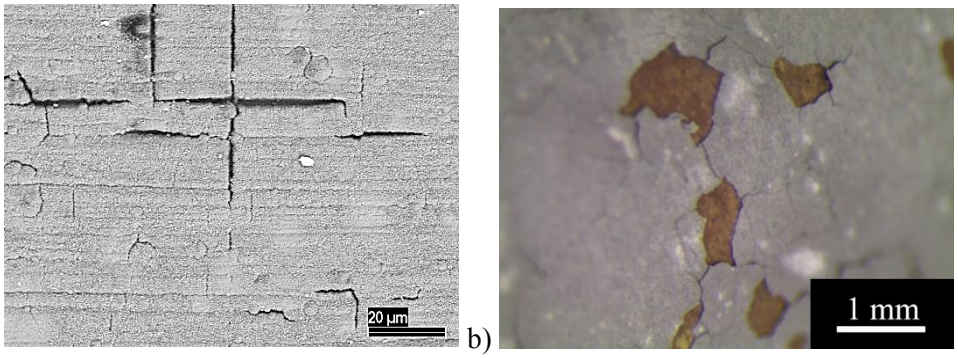

Figure 2. The destruction of chromium coatings on samples of alloy E110 o.ch. after high-temperature oxidation in pairs (HTO): a – 800 ºC, 5000 s (coating thickness 8-10 μm, SEM image), b – 1000 ºC, 5000 s (coating thickness 2-4 μm, optical image).

As can be seen from Figure 3, the coatings deposited had a characteristic multilayer structure. The total thickness of the protective layer in different modes was ~ (2–10) μm.

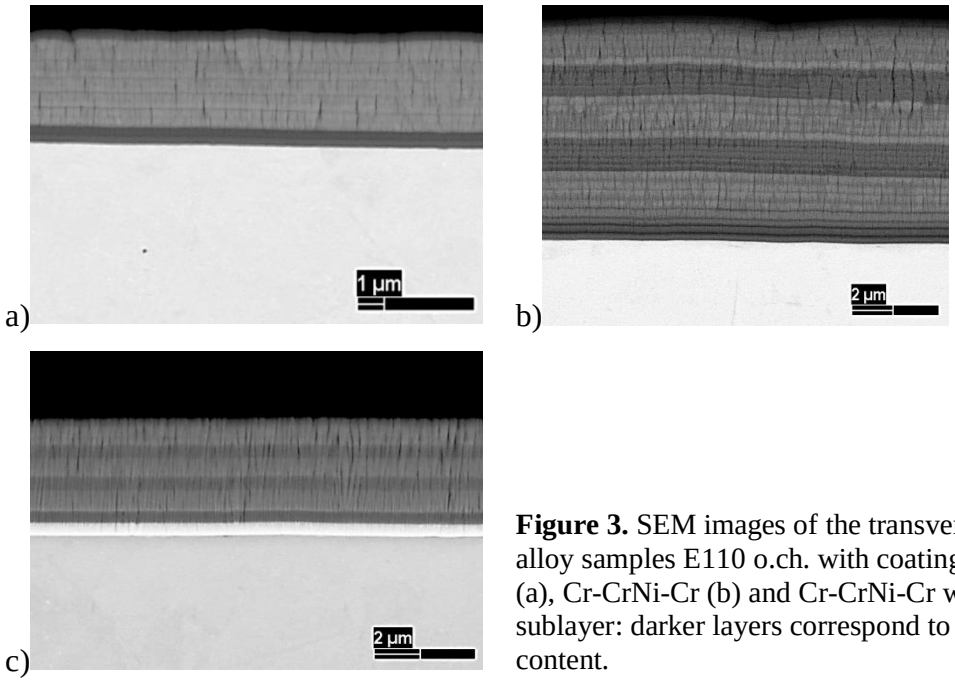

Figure 3. SEM images of the transverse structure of alloy samples E110 o.ch. with coatings Cr-FeCrNi-Cr (a), Cr-CrNi-Cr (b) and Cr-CrNi-Cr with the Mo (c) sublayer: darker layers correspond to an increased Cr content.

Analysis of the transverse structure of samples from alloy E110 o.ch. after oxidation at 1200 ºC with 500 s exposure showed that the structural phase state of the material is characterized by the presence of three distinct zones, which is consistent with the known results of other researchers [11]: ZrO_2 oxide zones near the outer and inner surfaces; an intermediate diffusion zone of α-Zr(O), which is essentially a solid solution of oxygen in zirconium stabilized in the α phase; “live” cross-section ex.β-Zr sample not affected by corrosive oxygen.

Oxide film on all samples has homogeneously dark gray color with no visible signs of destruction or shedding. As can be seen from Figure 4, the oxide layer on Zr-1% Nb alloy samples without coatings and with Cr-FeCrNi-Cr coatings has approximately the same thickness of 52±5 μm. There is

no thick oxide layer on samples with Cr-CrNi-Cr coatings and Cr-CrNi-Cr coatings with the Mo sublayer which indicates their high protective properties. It was shown that the presence of any coatings under study makes the α-Zr(O) zone structure more uniform and coarse-grained. Its thickness decreases from 85±5 μm for samples without coatings to 44±5 μm for samples with Cr-FeCrNi-Cr coatings and 33±5 μm for samples with Cr-CrNi-Cr coatings. No oxygen diffusion zone α-Zr(O) was detected on the samples with Cr-CrNi-Cr coatings and a Mo sublayer. It should be noted that samples with Cr-FeCrNi-Cr coatings have a weight gain of 12.0±0.5 mg·cm^{-2}, which is larger than that on the samples in the initial state 10.9±0.2 mg·cm^{-2}, which is associated with the active oxidation of coating elements, in particular Fe. Samples with Cr-CrNi-Cr coatings and Cr-CrNi-Cr coatings with the Mo sublayer have a significantly smaller gain of 6.6±0.5 mg·cm^{-2} and 6.1±0.5 mg·cm^{-2}, respectively.

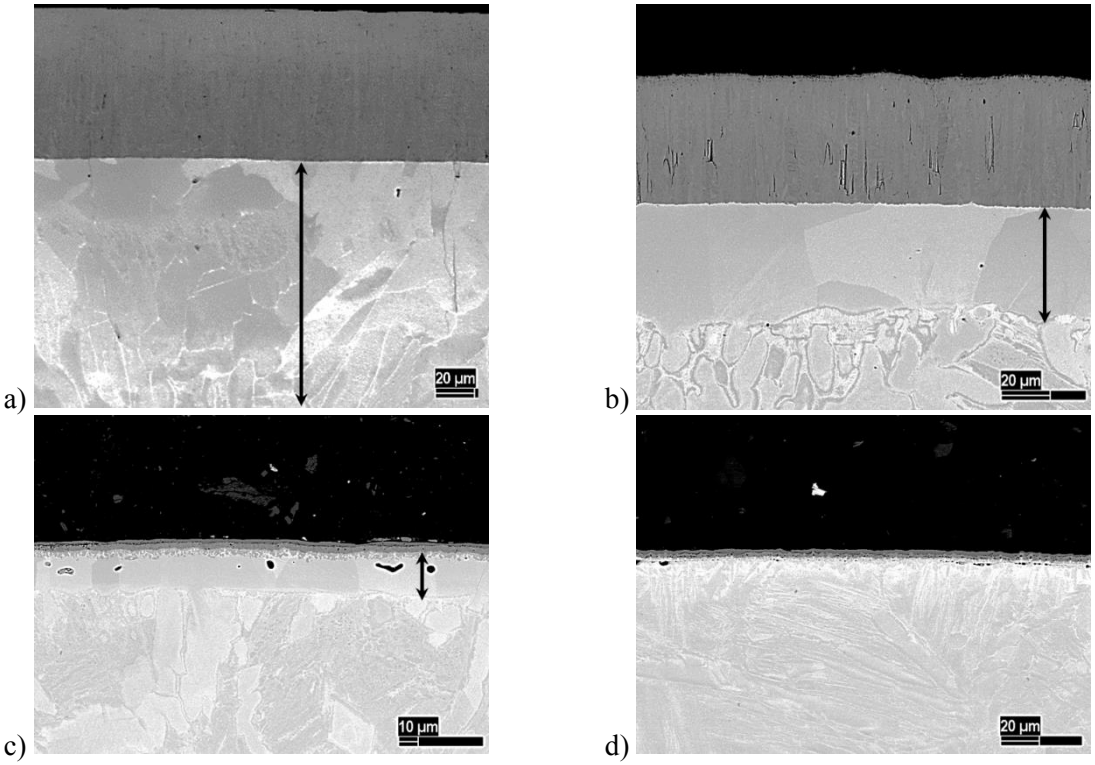

Figure 4. SEM images of the transverse structure of E110 o.ch. samples in the initial state (a) and with the coatings Cr-FeCrNi-Cr (b), Cr-CrNi-Cr (c) and Cr-CrNi-Cr with the Mo sublayer (after corrosion tests 1200 ºC 400 s: arrows indicate the α-Zr(O) region.

Elemental analysis of samples with Cr-FeCrNi-Cr coatings showed that the coating atoms are noticeably redistributed over the cross section of the sample as a result of exposure at high temperature in water steam. Fe and Cr atoms shown noticeably dissolving in the alloy under the oxides, along with participation in the formation of (FeCrNi)O_x, Cr_2O_3, Fe_mO_n oxides, and thereby slow down the diffusion of oxygen deep into the material, inhibiting oxidation, which can be seen from Figure 5. Moreover, an increased concentration of chromium atoms is observed up to depths of 100-120 μm, and iron - up to 200-300 μm, and then the signal goes to background values.

There are characteristic multiphase structures near the surface of the E110 o.ch. alloy shown at Figure 6, formed as a result of intense diffusion motion of atoms from the Cr-CrNi-Cr and Cr-CrNi-Cr coatings with the Mo sublayer: a dense Cr_2O_3 layer near the outer surface and transition regions with different contents of Zr, Cr, O, Mo (Tables 1 and 2), in particular, $ZrCr_2$ precipitates under that are found.

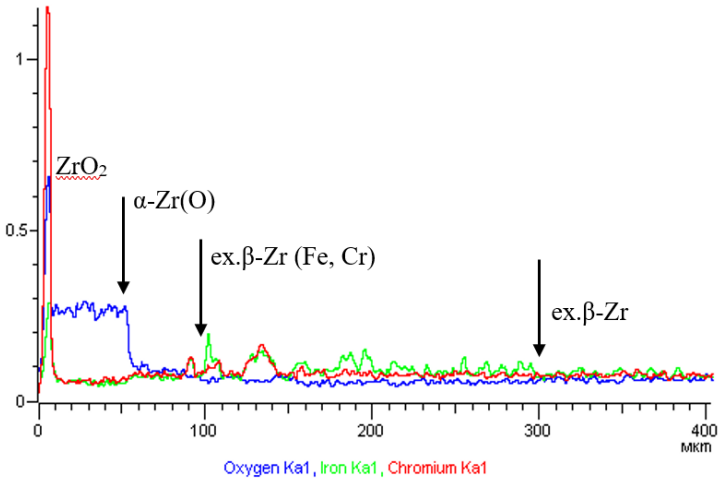

Figure 5. Fe, Cr, O distribution over the depth of a sample coated with Cr-FeCrNi-Cr after oxidation in steam at 1200 °C for 400 s: the arrows indicate the interface between ZrO_2, α-Zr(O), ex.β-Zr and the maximum penetration of Fe atoms (X-ray microanalysis data).

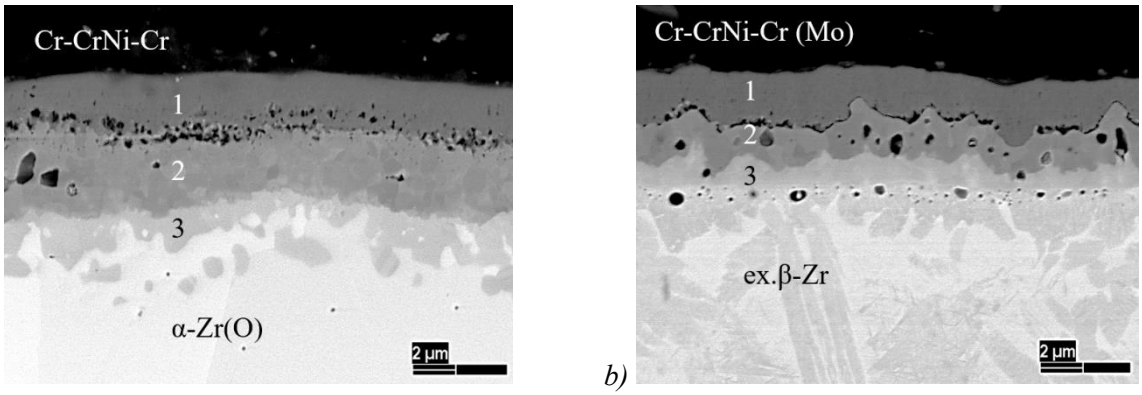

a) *b)*

Figure 6. Transverse structure of the E110 o.ch. alloy sample coated with Cr-CrNi-Cr (a) and Cr-CrNi-Cr with the Mo (b) sublayer after the HTO 1200 ºC 400 s: the numbers show the elemental composition measurement ranges in tables 1 and 2 respectively.

Table 1. The elemental composition of various regions of E110 o.ch. sample with Cr-CrNi-Cr coating after HTO 1200 ºC 400 s.

Measurement area	Element content, %		
	O	Cr	Zr
1 – Cr_2O_3	33.8	65.8	0.0
2 – Cr + Zr	0.0	98.0	2.0
3 – $ZrCr_2$ + O	1.2	50.7	45.9

Table 2. The elemental composition of various regions of E110 o.ch. sample with Cr-CrNi-Cr coating and Mo sublayer after HTO 1200 ºC 400 s.

Measurement area	Element content, %			
	O	Cr	Zr	Mo
1 – Cr_2O_3	35.6	64.4	0.0	0.0
2 – Cr + Zr	0.0	96.2	0.6	3.2
3 – Cr + Zr + Mo	0.0	37.9	48.4	13.7

Thus, the Mo barrier layer between E110 alloy and coating Cr-CrNi-Cr inhibits the dissolution of coating elements in sample material and blocks penetration of oxygen from high-temperature steam deep into the cladding effectively, preventing brittle α-Zr(O) phase formation. It became possible to save more than 100 μm of cladding live section in comparison with samples without coatings, which is clearly seen from Figure 7.

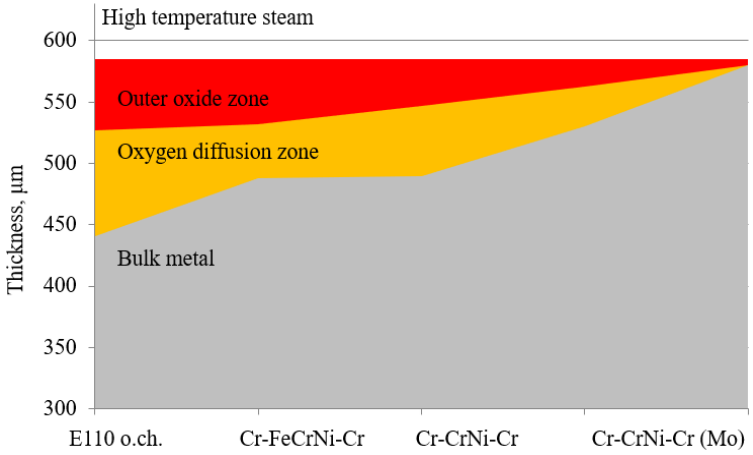

Figure 7. Schematic dependence of the cladding from E110 o.ch. live cross-section, retained after high-temperature oxidation in steam at 1200 °C for 400 s, depending on the type of coating deposited.

4. Conclusion

Protective coatings Cr-FeCrNi-Cr and Cr-CrNi-Cr for cladding tubes from E110 o.ch. alloy, effectively inhibit the oxygen penetration deep into the material during high-temperature tests at 1200 ºC with a up to 400 s exposure have been developed. It was shown that use of the Mo barrier layer allows to block oxygen diffusion and prevent the dissolution of coating elements in the sample material, thereby preserving more than 100 μm of the cladding live cross section.

Acknowledgements

This work was supported by Competitiveness Growth Program of the Federal Autonomous Educational Institution of Higher Education National Research Nuclear University MEPhI (Moscow Engineering Physics Institute).

References

[1] Kurt A 2018 *J. of Nuclear Materials* **501** 13–30
[2] Weiwei Xiao, Huiqin Chen, Xiaoshuang Liu et al. 2019 *J. of Nuclear Materials* **526** 151777
[3] Brachet J C, Idarraga I, Le Flem M et al. 2019 *J. of Nuclear Materials* **517** 26–285
[4] Park J.-H, Kim H.-G, Park J.-Y et al. 2015 *Surface and Coatings Technology* **280** 256–259
[5] Bischoff J, Delafoy C, Vauglin C et al. 2018 *Nuclear Engineering and Technology* **50** 223–228
[6] Kalin B A, Volkov N V, Valikov R A et al. 2014 *Bulletin of the Russian Academy of Sciences. Physics* **78** (6) 553–557
[7] Valikov R A, Yashin A S, Yakutkina T V et al. 2015 *J. of Physics: Conf. Ser.* **652** 012068
[8] Yashin A S, Safonov D A, Kalin B A et al. 2017 *IOP Conf. Series: J. of Physics: Conf. Series* **857** 012057
[9] Kalin B A, Volkov N V, Valikov R A et al. 2016 *IOP Conf. Series: J. of Physics: Conf. Series* **130** 012039
[10] Polunin K K, Urusov A A, Mokrushin A A, Soldatkin D M, Kuzma-Kichta Yu A, Kiselev D S, Bespechalov B N and Bazyuk S S 2018 *New in Russian Electrical Power Engineering* **9** 62–71
[11] Polunin K K, Urusov A A, Bazyuk S S, Kiselev D S and Kuzma-Kichta Yu A 2019 *J. Phys.: Conf. Ser.* **1370** 012050